Reprinted from Journal of the Optical Society of America B, Vol. 4, 1765, November 1987

Practical guide for $7S$ resonant frequency mixing in mercury: generation of light in the 230–185- and 140–120-nm ranges

A. V. Smith and W. J. Alford

Sandia National Laboratories, Albuquerque, New Mexico 87185

Received February 28, 1987; accepted June 22, 1987

We present recent measurements of refractive indices, nonlinear susceptibilities, and isotope shifts important for sum- and difference-frequency mixing through the $7^{1,3}S$ two-photon resonances of Hg. These data are presented in a form that makes it possible to make quick and accurate calculations of index-matching and mixing efficiencies in the low-intensity limit.

INTRODUCTION

Recent work by numerous researchers has demonstrated that atomic-mercury vapor is an attractive medium for the generation of vacuum-ultraviolet (VUV) light by sum-frequency mixing. For example, Bokor *et al.*[1] demonstrated parametric generation of VUV light at several frequencies by two-photon resonant pumping of the Hg $6D$ and $10S$ resonances. Tomkins and Mahon[2] achieved efficiencies approaching 1% at certain wavelengths while producing light over portions of the range 126–117 nm with the 7^1S state providing resonant enhancement. Hilbig and Wallenstein[3] used resonant enhancement from the 7^1S, 6^1D_2, and 7^1D_2 states to demonstrate sum- and difference-frequency mixing over portions of the range 196–109 nm. Similarly, Herman and Stoicheff[4] used the 8^1S and $7^{1,3}D$ resonances to enhance sum-frequency mixing over the range 105–87.5 nm.

Although the experimental results referenced above are most useful in demonstrating the utility of Hg as a nonlinear medium for VUV generation, a comparison of the experimental data with expected performance and optimization of the mixing efficiencies has been difficult because of the lack of knowledge of Hg atomic parameters such as nonlinear susceptibilities and refractive indices. We recently measured the refractive index[5] and nonlinear susceptibility[6] of Hg over the range 0–83 000 cm^{-1} for mixing through the $7^{1,3}S$ states. In addition, we studied the effects of isotope structure and amplified spontaneous emission[7] (ASE) on mixing efficiencies. These results make it possible to predict with confidence the index-matching requirements and mixing efficiencies under the assumption that effects due to higher-order nonlinearities are negligible. The purpose of this paper is to summarize our results in a form directly applicable to $7^{1,3}S$ resonantly enhanced sum- and difference-frequency mixing in Hg. We present plots from which the refractive-index mismatch and the nonlinear susceptibilities can be easily determined. By gathering much of what is known about those quantities crucial for third-order sum- and difference-frequency mixing in Hg in one place, we intend this report to be a practical guide for those interested in generating light in the 230–185- and 140–120-nm ranges.

The predictions of index-matching and conversion efficiencies presented here are accurate only in the low-intensity limit, where nonlinear refractive indices, parametric processes, ac Stark shifts, fifth-order mixing, reconversion, and other complicating processes can be ignored. To satisfy this requirement strictly, generally the input intensities should be 10^5 W/cm^2 or less. We acknowledge that much higher intensities are typical of most reports of Hg mixing in the literature; the results presented here will provide a starting point for optimizing mixing efficiencies and for investigating the roles of various higher-order processes. Equally important, these results make it possible to predict mixing efficiencies in the unfocused geometries necessary for systems that can be scaled to high energies.

BACKGROUND

Figure 1 is an energy-level diagram of Hg with a typical mixing scheme and frequency notation indicated. Usually ω_1 will be either half of the 7^1S energy at 313 nm or near the 6^3P resonance at 254 nm. Corresponding ω_2 values for 7^1S resonance will be 313 and 405 nm, respectively. For output wavelengths spanning 120–140-nm (71 400–83 300 cm^{-1}), ω_3 ranges from 1.33 μm to 516 nm for 7^1S and from 1.10 μm to 477 nm for 7^3S resonance. For difference-frequency generation over the range 230–185 nm, ω_3 ranges from 490 nm to 1.01 μm. All these wavelengths are readily generated by using pulsed dye lasers and standard nonlinear frequency mixing techniques. We have covered these ranges in the course of our measurements.

Mercury is a convenient mixing medium because of its high vapor pressure at moderate temperatures. The equilibrium vapor pressure of Hg versus temperature is plotted in Fig. 2. A variety of Hg hot cells for achieving Hg vapor pressures up to 10 Torr are described in Refs. 1–5. Both heat-pipe and hot-window cells have been used and are relatively simple to build and operate. Care must be taken to select VUV-quality output windows and to eliminate water vapor from the cell. Water vapor has strong, broad absorption bands in the range 120–140 nm with peak absorption coefficients of 1 cm^{-1}/Torr.[8]

Expressions relating the output power at ω_4 to input parameters and Hg properties are[9]

0740-3224/87/111765-06$02.00

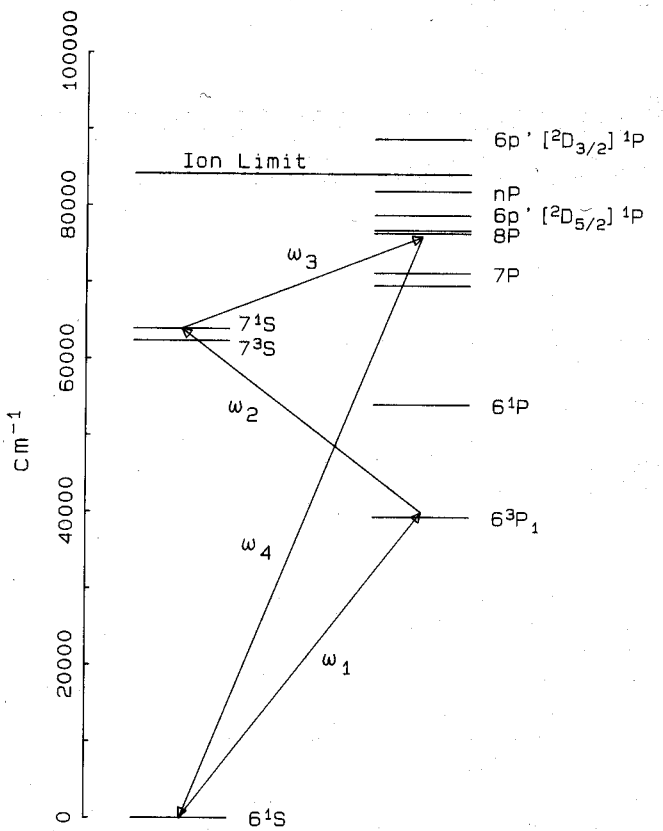

Fig. 1. Energy-level diagram of Hg and typical mixing scheme with notation indicated.

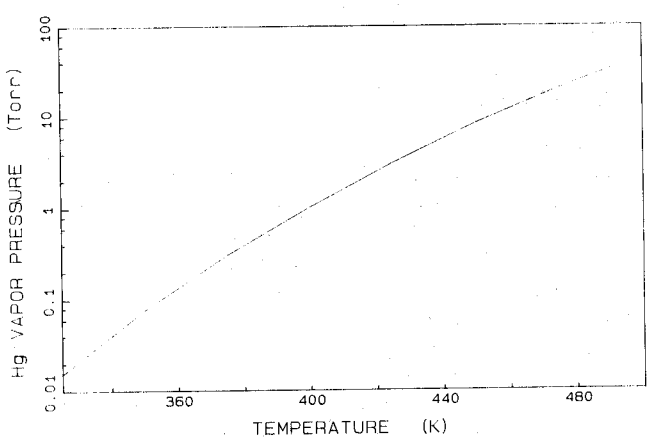

Fig. 2. Equilibrium vapor pressure of atomic Hg as a function of temperature.

$$P_4 = 1.9 \times 10^{-49}\,\mathrm{K}\,P_1P_2P_3 \times \left|\frac{\chi_p(\omega_1)\chi_p(\omega_4)\omega_4 NLS(\omega_1+\omega_2)\sin(NL\Delta k/2)}{A(NL\Delta k/2)}\right|^2 \quad (1)$$

and

$$P_4 = 7.8 \times 10^{-49}\,\mathrm{K}\,\omega_1\omega_2\omega_3\omega_4 P_1P_2P_3 \times |\chi_p(\omega_1)\chi_p(\omega_4)NFS(\omega_1+\omega_2)|^2, \quad (2)$$

$$K = \begin{cases} 1 & \text{for } \omega_1 \neq \omega_2 \\ 1/4 & \text{for } \omega_1 = \omega_2 \end{cases}, \quad (3)$$

where Eq. (1) applies for unfocused beams with a uniform spatial intensity profile of area A cm^2 and Eq. (2) holds for a tight-focus geometry (confocal parameter b much less than the cell length).

In these expressions, the powers P_ω are in watts, ω's are in inverse centimeters, N is the Hg atomic density in units of cm^{-3}, L is the interaction length in centimeters, Δk is the phase mismatch in units of cm^{-1}/(atom/cm^3), and $\chi_p(\omega)$ is in units of $(ea_0)^2$/cm^{-1}. $S(\omega_1+\omega_2)$ is a parameter that describes the shape of the two-photon resonance, and the function F depends on the index-matching conditions. The evaluation of F, Δk, the χ's, and $S(\omega_1+\omega_2)$ will be discussed in more detail below. Key assumptions of these expressions for P_4 are that there is no linear absorption at any of the four frequencies and that there is negligible depletion of the input waves. For focused beams, three coaxial input beams with Gaussian spatial intensity profiles and equal confocal parameters are assumed.

INDEX MATCHING

We now describe how one calculates the index mismatch for any set of wavelengths and discuss techniques for obtaining an optimum mismatch. The quantity Δk is the index mismatch and is defined as

$$\Delta k = [k(\omega_4) - k(\omega_1) - k(\omega_2) \pm k(\omega_3)]/N, \quad (4)$$

where the (lower) upper sign is for (sum-) difference-frequency mixing. The k's are the magnitudes of the wave vectors of the four frequencies in the Hg vapor.

The confocal parameter b, which is the length of the focal volume, is defined by

$$b = 16/k(\omega)\delta^2, \quad (5)$$

where δ is the full angle of the far-field diffraction cone.

For sum-frequency mixing, the function F in Eq. (2) is given by[10,11]

$$|F|^2 = \begin{cases} \pi^2(b\Delta kN)^2 \exp(b\Delta kN), & \Delta k < 0 \\ 0, & \Delta k \geq 0 \end{cases} \quad (6)$$

and has a maximum value of 5.34 when $b\Delta kN = -2$. For difference-frequency mixing, $|F|^2$ peaks at $b\Delta kN = 0$ with a maximum value that depends on the frequencies ω_1–ω_4. For the wavelength range of interest here the maximum value of $|F|^2$ is 5 ± 1, and $|F|^2$ falls approximately exponentially with $b\Delta kN$ to about half of its peak value for $|b\Delta kN| = 1$.

From Eqs. (1), (2), and (6), it is evident that for sum- and difference-frequency mixing with collimated beams and for difference-frequency mixing using focused beams, maximum output power P_4 occurs for $\Delta k = 0$, while for sum-frequency generation with focused beams, P_4 is maximized for $b\Delta k = -2$ and is zero for $\Delta k \geq 0$. In Fig. 3 we have plotted Δk_p or a partial Δk (from the data of Ref. 5), where

$$\Delta k_p(\omega) = [k(\omega) + k(E_{7S} - \omega)]/N, \quad (7)$$

$$k(-\omega) = -k(\omega), \quad (8)$$

so that

$$\Delta k = \Delta k_p(\omega_4) - \Delta k_p(\omega_1). \quad (9)$$

From this plot it is straightforward to determine Δk for any

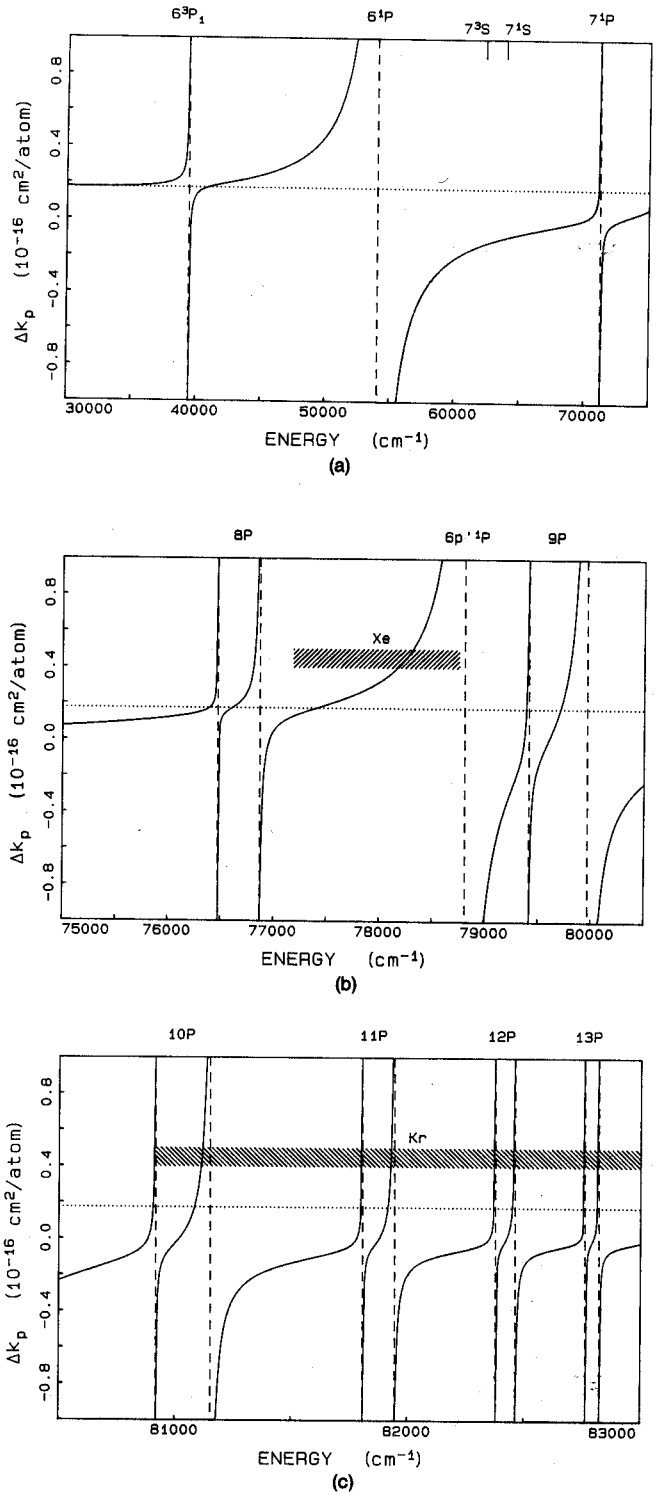

Fig. 3. Partial Δk (as defined in the text) as a function of frequency. Three energy ranges are given: (a) 30 000–75 000 cm^{-1}, (b) 75 000–80 500 cm^{-1}, (c) 80 500–83 000 cm^{-1}. Hatching indicates regions of negative dispersion for Xe and Kr buffer gases.

ω_4 with any set of input frequencies as long as $\omega_1 + \omega_2 = 63\,928\ cm^{-1}$, the energy of the 7^1S state. For example, for generation of 121.567-nm Lyman-α light using $\omega_1 = \omega_2 = 31\,964\ cm^{-1}$, ΔkN is $(-0.05\ cm^{-1}) - (+0.18\ cm^{-1})$ or $-0.23\ cm^{-1}$ for a Hg density of 10^{16} atoms/cm^3. Because the special case $\omega_1 = \omega_2$ is expected to find widest application, we have drawn dotted lines at 0.18×10^{-16}, the value of $\Delta k_p(\omega_1)$ for this case. For $\omega_1 = \omega_2$, Δk is positive for frequencies ω_4 where the solid lines lie above the dotted lines.

The hatched regions indicate ranges where Δk of Xe or Kr is negative.[12] An examination of this plot reveals that by using mixtures of the rare gases and Hg to index match, and with $\omega_1 = \omega_2 = 31\,964\ cm^{-1}$, one can index match over more than 90% of the range 140–120 nm. Notable exceptions are wavelengths near the Hg $8P$ and $9P$ levels. For example, for $\omega_4 = 76\,795\ cm^{-1}$, one of the resonance lines of atomic oxygen, $\Delta k = (0.36\ cm^{-1}) - (0.18\ cm^{-1}) = 0.18\ cm^{-1}$ at 10^{16} atoms/cm^3. This mismatch cannot be compensated for by using a rare-gas buffer. However, $\Delta k = 0$ can be achieved for this frequency by selecting for ω_1 the value where $\Delta k_p(\omega_1) = 0.36 \times 10^{-16}$. This occurs at $\omega_1 = 39\,210\ cm^{-1}$. In general, by tuning ω_1 near one of the $6P$ levels, one can index match at any desired output frequency ω_4.

Another means of varying Δk for unfocused beams is to cross the beams at a slight angle. For $\omega_1 = \omega_2$, this introduces an additional contribution to Δk given by[5]

$$\Delta k_{\text{cross}} = \frac{\pm k_1 k_3}{2k_1 + k_3}\theta_2, \tag{10}$$

where the (upper) lower sign is for (sum-) difference-frequency mixing. This refractive-index mismatch should be added to the Δk calculated from Fig. 3. This permits compensation of (negative) positive Δk for (sum-) difference-frequency mixing. Thus, for example, with $\omega_2 = \omega_1$ and unfocused beams, difference-frequency mixing can be index matched over the entire range 230–185 nm by crossing the input beams at a small angle. At Hg densities of a few Torr, useful angles are typically $<1°$.

Finally, we note that, for maximum conversion efficiency, index matching must be maintained over the entire conversion length. Thus, if index matching is done using rare-gas–Hg mixtures, uniform densities must be maintained along the entire mixing length. This is an important consideration in the design of the Hg hot cell.

Although we have focused our attention on index matching for two-photon resonance with the 7^1S state, the same procedures apply for 7^3S resonance, and the $\Delta k_p(\omega)$ curve is not distinguishable on the scale of the plot of Fig. 3.

SUSCEPTIBILITIES

Having addressed the question of optimizing index matching, we now consider the evaluation of the nonlinear susceptibilities, χ_p, that appear in Eqs. (1) and (2). Since we are concerned with two-photon resonant processes, it is convenient to split the third-order nonlinear susceptibility into the three parts, $\chi_p(\omega_1)$, $\chi_p(\omega_4)$, and $S(\omega_1 + \omega_2)$, that appear in Eqs. (1) and (2). We define $\chi_p(\omega)$ by

$$\chi_p(\omega) = \sum_f \left(\frac{\langle i|\mathbf{d}\cdot\hat{e}_{\omega'}|f\rangle\langle f|\mathbf{d}\cdot\hat{e}_{\omega}|g\rangle}{\omega_f - \omega} + \frac{\langle i|\mathbf{d}\cdot\hat{e}_{\omega}|f\rangle\langle f|\mathbf{d}\cdot\hat{e}_{\omega'}|g\rangle}{\omega_f - \omega'} \right), \tag{11}$$

where $\omega + \omega' = E_i = 63\,928\ cm^{-1}$ ($62\,350\ cm^{-1}$) for the 7^1S (7^3S) resonance. Here the $\hat{e}_{\omega'}$'s are unit vectors defining the polarization of light at frequencies ω, and d is the dipole-

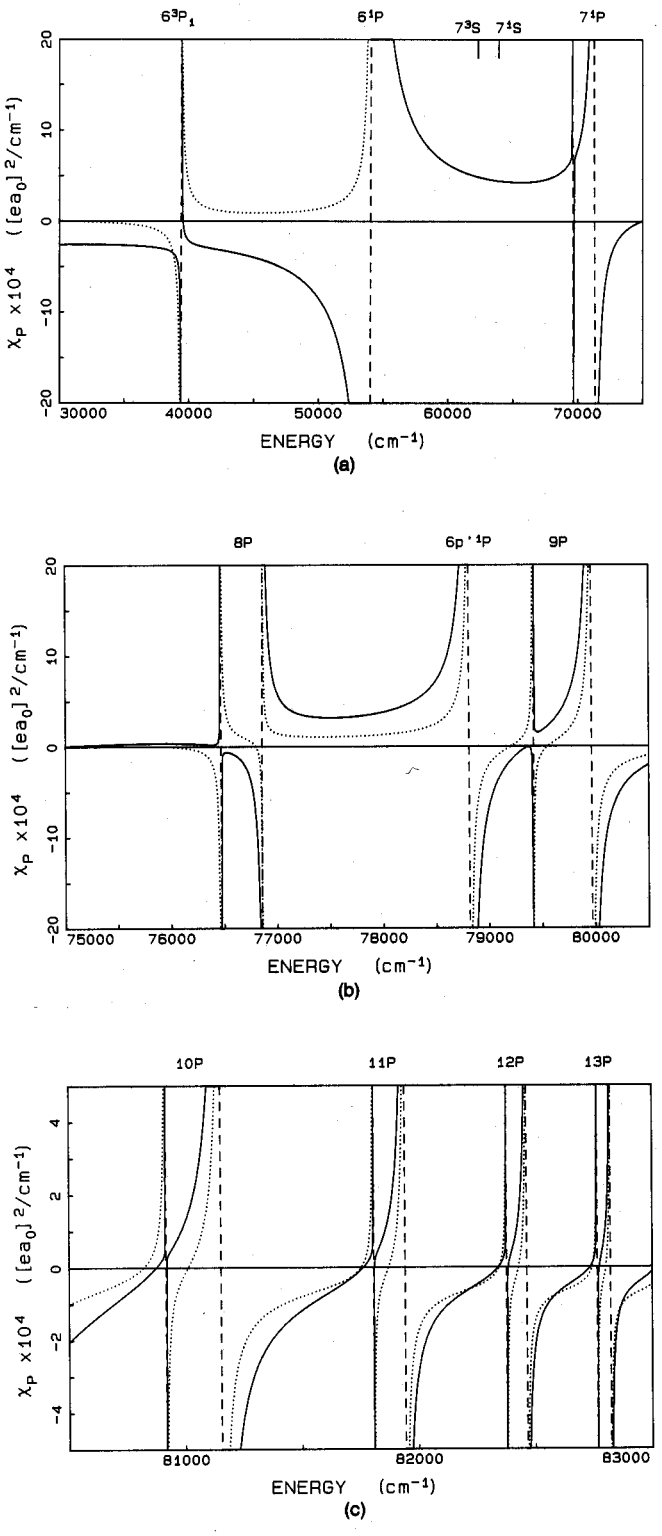

Fig. 4. Partial susceptibilities χ_p (as defined in the text) as a function of frequency. Solid lines are for 7^1S resonance; dotted lines are for 7^3S resonance. Three energy ranges are given: (a) 30 000–75 000 cm^{-1}, (b) 75 000–80 500 cm^{-1}, (c) 80 500–83 000 cm^{-1}.

moment operator. The $\chi_p(\omega)$'s are measured in units of $(ea_0)^2/cm^{-1}$. The relation between the standard definition of third-order susceptibility[9] $\chi^{(3)}(-\omega_4; \omega_1, \omega_2, \omega_3)$ and $\chi_p(\omega_1)\chi_p(\omega_4)$, and $S(\omega_1 + \omega_2)$ is

$$\chi^{(3)}(-\omega_4; \omega_1, \omega_2, \omega_3) = \frac{(ea_0)^4}{6(hc)^3} S(\omega_1 + \omega_2)\chi_1\chi_p(\omega_4)$$
$$= 8.87 \times 10^{-25} S(\omega_1 + \omega_2)\chi_1\chi_p(\omega_4), \quad (12)$$

where cgs units are used, so $\chi^{(3)}$ has dimensions of cm^6/erg.

$\chi_p(\omega_1)$ and $\chi_p(\omega_4)$ are plotted in Fig. 4. These plots are used much like the Δk plots, with $\chi_p(\omega_4)$ and $\chi_p(\omega_1)$ read directly from the plot of χ_p at frequencies ω_4 and ω_1, respectively. The solid lines are for resonance with the 7^1S level, and the dotted lines are for resonance with the 7^3S level. We have assumed linear polarizations of all waves. For 7^1S resonance, ω and ω' (i.e., ω_1 and ω_2 or ω_3 and ω_4) are polarized parallel, while for 7^3S resonance ω and ω' have perpendicular polarizations. These choices are dictated by atomic-dipole transition selection rules. The plotted curves also apply for circular polarization of ω and ω', with the appropriate polarizations readily determined from atomic selection rules. In either case, the two matrix-element products in Eq. (11) have the same sign for 7^1S resonance and opposite signs for 7^3S resonance. Thus, for mixing through the 7^3S resonance with $\omega \approx \omega'$, near cancellation occurs, and χ_p is small and goes to zero for $\omega = \omega' = 31\,175\ cm^{-1}$. This is apparent in the plot of χ_p. Hence mixing through 7^1S is possible with $\omega_1 = \omega_2$; but mixing through 7^3S requires three distinct input frequencies.

Because of the large uncertainty in the susceptibility between 55 000 and 76 000 cm^{-1} for the 7^3S resonant case,[6] we have omitted that part of the curve.

TWO-PHOTON RESONANCE LINE SHAPE

The function $S(\omega_1 + \omega_2)$ describes the shape of the two-photon resonance. For a single Doppler-broadened Lorentzian line of homogeneous half-width Γ, it is easy to show that $S(\omega_1 + \omega_2)$ is given by

$$S(\omega_1 + \omega_2) = \frac{1}{w\pi^{1/2}} \int \frac{\exp(-x_2)}{x - \zeta}\, dx = Z(\zeta)/w, \quad (13)$$

$$\zeta = (\omega_1 + \omega_2 - \omega_{7S} + i\Gamma)/w, \quad (14)$$

$$w = \omega_{7S}\,(2kT/mc^2)^{1/2} = \Delta\omega_D/2(\ln 2)^{1/2}, \quad (15)$$

where $Z(\zeta)$ is the plasma dispersion function,[13] $\Delta\omega_D$ is the Doppler width of the $7S$ transition (FWHM), and m is the Hg atomic mass. $S(\omega_1 + \omega_2)$ is maximum at line center, and for $\Gamma \ll \Delta\omega_D$ its maximum value is $1.77/\Delta\omega_D$. For a typical Hg $7S$ Doppler width of 0.067 cm^{-1}, corresponding to a Hg temperature of 155°C, $|S|^2_{max} = 1940\ cm^2$. This holds only for lasers of linewidth much less than the Doppler width $\Delta\omega_D$. For laser widths $\Delta\omega_L$ comparable with $\Delta\omega_D$, a reasonable approximation is to replace $\Delta\omega_D$ with $[(\Delta\omega_D)^2 + (\Delta\omega_L)^2]^{1/2}$.

In fact, the $7S$ two-photon resonances are not Doppler-broadened single Lorentzians but are complicated by the presence of six abundant isotopes in naturally occurring Hg. The actual $|S(\omega_1 + \omega_2)|^2$'s, shown as dotted lines in Fig. 5, are calculated by replacing the single resonance in Eq. (13) by the appropriately weighted and shifted isotopic resonances. A natural isotopic mixture is assumed with a $7S$ Doppler

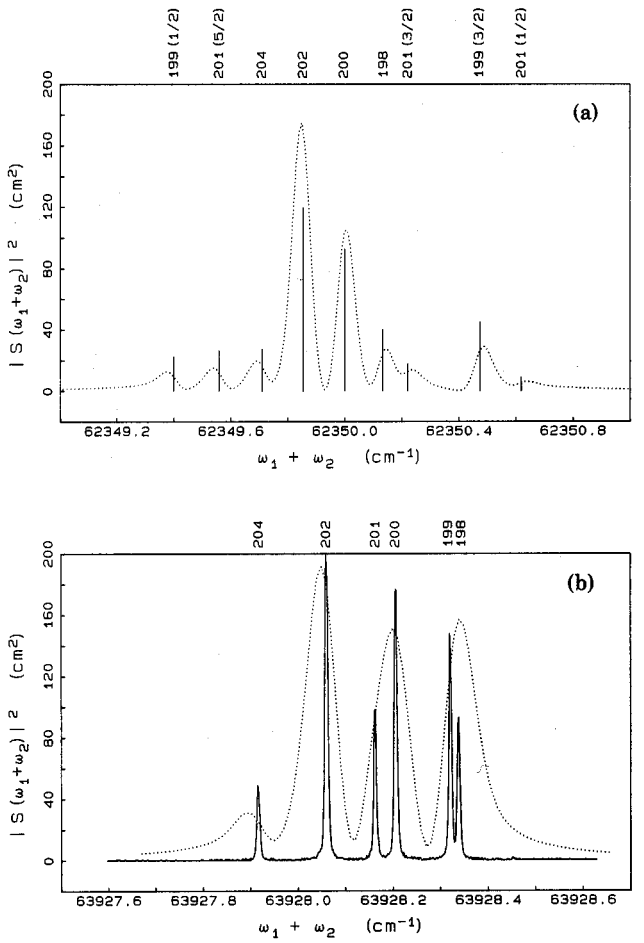

Fig. 5. The two-photon resonance line-shape function $|S(\omega_1 + \omega_2)|^2$ for (b) the 7^1S and (a) the 7^3S resonances. The solid lines in (a) indicate calculated positions and strengths of the various Hg isotopes with unknown constant frequency offset. The solid line is a Doppler-free fluorescence spectrum of the 7^1S resonance for a natural Hg isotopic mixture. Line positions are accurate to <0.01 cm^{-1}.

width of 0.067 cm^{-1}. The upper plot is for the 7^3S resonance, and the lower is for the 7^1S resonance. The vertical lines in Fig. 5(a) indicate the calculated line-center positions and relative strengths of the various isotopes and, for odd masses, their hyperfine components, based on the data of Ref. 14. The isotopic mass (with the F quantum number for 7^3S in parentheses for hyperfine components) for each peak is shown at the top of each plot. The solid curve in Fig. 5(b) is a Doppler-free absorption spectrum that we obtained by using a narrow-linewidth laser with counterpropagating circularly polarized beams and observing the fluorescence from the 7^1S level.[7] This Doppler-free fluorescence spectrum confirms the shifts calculated for the various isotopes from the data of Ref. 14 for 7^1S and, in addition, provides an absolute frequency scale for the transitions accurate to better than 0.01 cm^{-1}. The important point is that the calculated maximum of $|S(\omega_1 + \omega_2)|^2$ for 7^1S at 63 928.05 cm^{-1} for a natural isotopic mixture is about 195, which is lower than that calculated for a single isotope by a factor of 10. The effect on the 7^3S is comparable in that the peak value of $|S|^2$ is about 180 cm^2. The 7^3S resonance profile has not been measured, however, so there is an unknown constant offset in the indicated line positions.

We have verified the shape of the dotted curve in Fig. 5(b) in detail at low mixing intensities.[7] Using the same narrow-linewidth lasers used in obtaining the Doppler-free spectrum and setting $\omega_1 = \omega_2 = 31\,964\ cm^{-1}$ and $\omega_3 = 18\,792\ cm^{-1}$, we generated the difference frequency of 45 136 cm^{-1} (221.6 nm) using crossed beams to index match. The resonance profile of the 221.6-nm intensity was measured by tuning ω_1 across the 7^1S resonance.

DISCUSSION

With the information presented above we can predict mixing efficiencies in the low-intensity limit. We compared such a prediction with measured mixing efficiencies in difference-frequency mixing through the 7^1S resonance to generate 221.6-nm light as described above. We find that for input intensities $<10^5$ W/cm^2, the observed 221.6-nm signal agreed with that predicted to within the observational uncertainty of a factor of 2.

At higher intensities we find that the shape of $|S(\omega_1 + \omega_2)|^2$ plotted in Fig. 5 no longer applies. At intensities above 10^5 W/cm^2 sufficient population is built up in the $7S$ state to initiate stimulated emission to the $6P$ levels. This ASE radiation power broadens the $6S$–$7S$ two-photon transition and hence modifies $S(\omega_1 + \omega_2)$. This effect will be discussed in more detail in a later publication.[7] At still higher intensities, additional nonlinear processes will become important. For example, at intensities of 10^7 W/cm^2, ac Stark shifts become comparable with the Doppler width. At 10^{10} W/cm^2, typical of focused beams, the role of higher-order effects can become overwhelming, and describing the mixing in terms of the third-order processes considered here may be inappropriate.[15] This is apparent in the results of Hilbig and Wallenstein,[3] for example, where strong sum-frequency signals are generated even in regions where Δk is strongly positive. In general, however, it appears that even at these high intensities the mixing efficiency has the same general shape as the $\chi_p(\omega_4)$ plotted in Fig. 4. This is evident, for example, in the results of both Refs. 2 and 3.

SUMMARY

In summary, we have presented much of the information necessary to calculate index-matching conditions and conversion efficiencies in the low-intensity limit for four-wave sum- and difference-frequency mixing in Hg over a broad and important region of the spectrum. Some of the expressions given here break down at high intensities, but that does not diminish their importance for collimated beam geometries such as would be necessary for systems scalable to high energies or as a starting point for optimizing mixing in focused geometries. The equations and data presented have been tested for the generation of 222-nm light by difference-frequency mixing through the 7^1S state using narrow-linewidth lasers at intensities $<10^5$ W/cm^2 and agree with observed conversion efficiencies within the factor-of-2 uncertainty in the measurements. We trust that by making the appropriate data on Hg readily accessible in an easy-to-

use form this paper will be useful as a starting point for those wishing to generate VUV light by nonlinear mixing in Hg.

ACKNOWLEDGMENTS

We thank Peter Esherick for his help in measuring the isotopic shifts and line shapes and J. W. Clements for technical support in all the experimental work.

This research was performed at Sandia National Laboratories and was supported by the U.S. Department of Energy under contract DE-AC04-76DP00789 for the Office of Basic Energy Sciences.

REFERENCES AND NOTES

1. J. Bokor, R. R. Freeman, R. L. Panock, and J. C. White, "Generation of high-brightness coherent radiation in the vacuum ultraviolet by four-wave parametric oscillation in mercury vapor," Opt. Lett. **6,** 182–184 (1981).
2. F. S. Tomkins and R. Mahon, "High-efficiency four-wave sum and difference mixing in Hg vapor," Opt. Lett. **6,** 179–181 (1981); R. Mahon and F. S. Tomkins, "Frequency up-conversion to the VUV in Hg vapor," IEEE J. Quantum Electron. **QE-18,** 913–920 (1982); F. S. Tomkins and R. Mahon, "Generation of continuously tunable narrow-band radiation from 1220 to 1174 Å in Hg vapor," Opt. Lett. **7,** 304–306 (1982).
3. R. Hilbig and R. Wallenstein, "Resonant sum and difference frequency mixing in Hg," IEEE J. Quantum Electron. **QE-19,** 1759–1770 (1983).
4. P. R. Herman and B. P. Stoicheff, "Tunable extreme-ultraviolet radiation from 105 to 87.5 nm using Hg vapor," Opt. Lett. **10,** 502–504 (1985).
5. A. V. Smith and W. J. Alford, "Vacuum ultraviolet oscillator strengths of Hg measured by sum-frequency mixing," Phys. Rev. A **33,** 3172–3180 (1986).
6. W. J. Alford and A. V. Smith, "Measured third-order susceptibilities and excited state oscillator strengths for atomic mercury," Phys. Rev. A **36,** 641–648 (1987).
7. A. V. Smith, G. R. Hadley, P. Esherick, and W. J. Alford, "Efficient two-photon resonant frequency conversion in Hg: the effects of amplified spontaneous emission," submitted to J. Opt. Soc. Am. B.
8. K. Watanabe and M. Zelikoff, "Absorption coefficients of water vapor in the vacuum ultraviolet," J. Opt. Soc. Am. **43,** 753–755 (1953).
9. J. F. Rientjes, *Nonlinear Optical Parametric Processes in Liquids and Gases* (Academic, New York, 1984).
10. J. F. Ward and G. H. C. New, "Optical third harmonic generation in gases by a focused laser beam," Phys. Rev. **185,** 57–72 (1969).
11. G. C. Bjorklund, "Effects of focusing on third-order nonlinear processes in isotropic media," IEEE J. Quantum Electron. **QE-11,** 287–296 (1975).
12. R. Mahon, T. J. McIlrath, V. P. Myerscough, and D. W. Koopman, "Third-harmonic generation in argon, krypton, and xenon: bandwidth limitations in the vicinity of Lyman-α," IEEE J. Quantum Electron. **QE-15,** 444–451 (1979).
13. B. D. Fried and S. D. Conte, *The Plasma Dispersion Function* (Academic, New York, 1961).
14. S. Gerstenkorn, J. J. Labarthe, and J. Vergès, "Fine and hyperfine structures and isotope shifts in the arc spectrum of mercury," Phys. Scr. **15,** 167–172 (1977).
15. See Chap. 4 of Ref. 9 for a discussion of efficiency-limiting processes.